The Canadian Mineralogist
Vol. 43, pp. 1631-1641 (2005)

THE APPLICATION OF HRTEM TECHNIQUES AND NANOSIMS TO CHEMICALLY AND ISOTOPICALLY CHARACTERIZE *GEOBACTER SULFURREDUCENS* SURFACES

MOSTAFA FAYEK§

Department of Earth and Planetary Sciences, University of Tennessee, Knoxville, Tennessee 37996, and Chemical Sciences Division, Oak Ridge National Laboratory, Oak Ridge, Tennessee 37831, USA

SATOSHI UTSUNOMIYA

Department of Geological Sciences, University of Michigan, Ann Arbor, Michigan 48109–1063, USA

SUSAN M. PFIFFNER AND DAVID C. WHITE

Centre for Biomarker Analysis, University of Tennessee, Knoxville, Tennessee 37932, USA

LEE R. RICIPUTI

Chemical Sciences Division, Oak Ridge National Laboratory, Oak Ridge, Tennessee 37831, and Department Earth and Planetary Sciences, University of Tennessee, Knoxville, Tennessee 37996, USA

RODNEY C. EWING

Department of Geological Sciences, University of Michigan, Ann Arbor, Michigan 48109–1063, USA

LAWRENCE M. ANOVITZ

Department Earth and Planetary Sciences, University of Tennessee, Knoxville, Tennessee 37996, and Chemical Sciences Division, Oak Ridge National Laboratory, Oak Ridge, Tennessee 37831, USA

FRANK J. STADERMANN

Department of Physics, Washington University, Saint Louis, Missouri 63130, USA

ABSTRACT

Bioprecipitated minerals are typically at the nanometer scale, hydrous, and beam-sensitive (*i.e.*, can recrystallize during analysis), making them difficult to characterize using standard spectroscopic or electron-beam techniques. We have combined the ion-imaging capabilities of nanoscale secondary-ion mass spectrometry (NanoSIMS) and advanced high-resolution transmission electron microscopy (HRTEM) in order to characterize the surfaces of *Geobacter sulfurreducens* and the bioprecipitated uranium phases. Our results reveal the association between nutrient uptake and precipitation of uranium minerals. Biosequestration of uranium is enhanced by addition of nutrients such as acetic acid, and uranium is precipitated on the surface of the bacteria as nanocrystals of uraninite (UO_2). The bioprecipitation of this anhydrous U-rich phase is significant; although UO_2 is thermodynamically stable over a range of pH values (2 to 12) and oxidizing conditions [Eh 0.2 to –0.2, or $\log f(O_2)$ of approximately –50 to –125], thermodynamic models of inorganic systems suggest that U^{6+} oxyhydroxide minerals should be stable. Our results suggest that the biofilm shielded the UO_2 from re-oxidation and that bacteria can immobilize uranium for extended periods, even under relatively oxidizing conditions in the subsurface.

Keywords: nanoscale secondary-ion mass spectrometry (NanoSIMS), high-resolution transmission electron microscopy (HRTEM), *Geobacter sulfurreducens*, uraninite.

§ *E-mail address*: mfayek@utk.edu

Sommaire

Les minéraux bioprécipités sont typiquement nanométriques, hydratés, et sensibles au faisceau, qui peut donc induire une recristallisation, ce qui les rend difficiles à caractériser au moyen de techniques standards d'analyse spectroscopique ou avec un faisceau d'électrons. Nous avons pu combiner les capacités d'imager à une échelle nanométrique au moyen de la spectrométrie de masse avec ions secondaires (NanoSIMS) et une technique avancée de microscopie électronique à transmission à haute résolution (HRTEM) afin de caractériser les surfaces *de Geobacter sulfurreducens* et de la phase uranifère bioprécipitée. Nos résultats révèlent une association entre l'ingestion de nutriments et la précipitation de minéraux uranifères. La bioséquestration de l'uranium est favorisée par l'addition de nutriments tels l'acide acétique, et l'uranium est précipité sur la surface des bactéries sous forme de cristaux nanométriques d'uraninite (UO_2). La bioprécipitation de cette phase uranifère anhydre est importante; quoique la phase UO_2 est thermodynamiquement stable sur un intervalle de valeurs de pH (de 2 à 12) et de conditions oxydantes [Eh de 0.2 à –0.2, ou log $f(O_2)$ d'environ –50 à –125], les modèles thermodynamiques de systèmes inorganiques semblent montrer que ce sont les minéraux oxyhydroxydés à U^{6+} qui devraient être stables. Nos résultats font penser que la biopellicule a protégé le UO_2 d'une ré-oxydation et que les bactéries peuvent immobiliser l'uranium pour des périodes prolongées, même sous conditions souterraines relativement oxydantes.

(Traduit par la Rédaction)

Mots-clés: spectrométrie de masse avec ions secondaires (NanoSIMS), microscopie électronique à transmission à haute résolution, *Geobacter sulfurreducens,* uraninite.

Introduction

Uranium biomineralization is an important consideration in environmental remediation of uranium mill tailings and other contaminated sites. There has been increasing interest in the processes involved in microbial uptake of uranium and other radionuclides (*e.g.,* Lovley *et al.* 1991, Gorby & Lovley 1993, Fein *et al.* 1997, Abdelouas *et al.* 1999, Suzuki & Banfield 1999, Southam 2000, Fowle *et al.* 2000, Kelly *et al.* 2002, Suzuki *et al.* 2002). For example, micro-organisms can physically remove radionuclides from solution through either bio-accumulation or biosorption (*e.g.,* Tsezos & Volesky 1982, Scharer & Byerley 1989). In bio-accumulation, radionuclides, such as uranium, are transported through the cell wall and sequestered. In biosorption, positively charged radionuclide ions are sequestered through adsorption onto the negatively charged functional groups found on most bacterial cell surfaces (*e.g.,* Suzuki & Banfield 1999, Southam 2000). These functional groups serve as nucleation sites for the precipitation of various radionuclide-bearing phases. Several studies have shown that the type of functional group responsible for the adsorption of aqueous uranium species on the bacterial cell wall is a function of the pH (Fowle *et al.* 2000, Fowle & Fein 2001, Kelly *et al.* 2002).

Although numerous studies have documented the presence of mineral-forming bacteria in a variety of environments (*e.g.,* Ferris *et al.* 1988, Konhauser *et al.* 1994, Abdelouas *et al.* 1999, Suzuki *et al.* 2002), few investigations have directly characterized the surface of the bacteria and biominerals (*e.g.,* Suzuki *et al.* 2002). The ability to visualize and track the uptake of radionuclides by micro-organisms with high spatial resolution is essential to gain an understanding of radionuclide–bacteria interactions. However, making measurements under physiological conditions needed to understand the role of elements and molecules in cells is challenging. Traditional analytical approaches rely on bulk or micrometer-scale measurements that either do not have the resolution required to correlate elemental distributions with specific cellular features, or require sample preparation techniques that can alter the original elemental distribution and chemical composition of the biological samples. For example, aqueous chemical fixation and embedding biological samples in plastics or epoxies can destroy the original chemical composition of the cells and have been shown to cause redistribution of elements such as Na, Ca and K (Chandra *et al.* 2000). In addition, biominerals are generally hydrous, electron-beam-sensitive (*i.e.,* can recrystallize or break down during analysis) and are very small in size (<100 nm), making them particularly difficult to characterize using standard spectroscopic or electron-beam techniques (*e.g.,* Suzuki & Banfield 1999). For example, XRD analysis of a heat-dried biomass showed that the uranyl-loaded samples contain crystalline ammonia uranyl phosphate (Andres *et al.* 1993), which has a crystal structure similar to the naturally occurring mineral uramphite (Markovic *et al.* 1988). However, it is not clear whether the uranyl phosphate formed by biosorption or during drying and sample preparation.

The objectives of this study are to image the surfaces of bacteria and correlate the uptake of radionuclides and nutrients while minimizing damage to the cells and biominerals. To achieve our objectives, *Geobacter sulfurreducens* were grown on Si wafers in the presence of U-rich (~200 ppm) synthetic groundwater. The biofilms were then freeze-dried to minimize damage and provide undisturbed samples. Isotopically labeled (^{13}C) acetic acid was used as a nutrient so that

nutrient and radionuclide uptake could be correlated. Ion imaging by secondary-ion mass spectroscopy (SIMS), (*e.g.,* Ramseyer *et al.* 1984, Chandra *et al.* 1986, 2000, Pacholski & Winograd 1999) was used to show the association between nutrient uptake and uranium sequestration. SIMS, in particular the NanoSIMS, is ideally suited for studies of elemental and isotopic gradients and the localization of isotopically labeled molecules, and NanoSIMS is the only technique available that can measure isotopic distributions with both high sensitivity (ppm) and high spatial resolution (*i.e.,* 50–1000 nm), produce images of single cells, and analyze a cell in three dimensions (*e.g.,* Hindié 1997, Chandra *et al.* 2000, Lechene *et al.* 2003). Advanced techniques of transmission electron microscopy (TEM), which can provide compositional and structural details at the nanoscale (*e.g.,* Utsunomiya & Ewing 2003) were used to visualize and track the uptake of uranium and to determine the structure of the bioprecipitated uraniferous minerals.

Methods

Experimental procedure

G. sulfurreducens cultures were prepared by Dr. Yuri Gorbi at Pacific North West National Laboratory using techniques described in detail by Lovley & Phillips (1988). Experiments consisted of growing a *G. sulfurreducens* biofilm on 2.5-cm Si wafers in the presence of U-rich synthetic groundwater. The Si wafers are necessary because they conduct electricity, which is required for ion imaging of biofilms by SIMS (see below; *e.g.,* Chandra *et al.* 1986, Chandra & Morrison 1997).

We first prepared the synthetic groundwater by dissolving 109 mg of $MgCl_2$, 6 mg KCl, 2 mg $MnCl_2$, and 0.12 g $NaHCO_3$ added to 500 mL of distilled water. A 200 ppm solution of UCl_4 was prepared under oxic conditions separately by dissolving 50 mg of UCl_4 powder in 250 mL of distilled water. The resulting solution had a yellow color, indicating that the uranium in solution was largely in the 6+ state, whereas aqueous solutions of U^{4+} are generally green. A HEPES-buffered growth medium, pH = 7, also was provided by Dr. Gorbi. A solution consisting of 67 μg of ^{13}C-labeled acetic acid in 13 mL of distilled water was then prepared and buffered, using the HEPES-buffered growth medium so that the final pH was 6.1. Next, test tubes, Si wafers, and solutions were autoclaved for 20 min. at 120°C to remove organic compounds. The *G. sulfurreducens* cells were then centrifuged at 2500 rpm for 20 min. at 10°C, and the supernatant solution was decanted. The test tubes were allowed to cool to room temperature and were placed in a nitrogen-rich atmosphere along with cells and liquids. A solution consisting of 87.5 mL of groundwater, 34 mL of 200 ppm UCl_4 solution, and 13.5 mL of the labeled acetic acid solution was then prepared, and *G. sulfurreducens* cells were suspended in 5 mL of the resultant solution. Two milliliters of this solution was then injected into the sterilized test tubes containing the Si wafers, and the tubes were placed in a 30°C temperature controlled oven to incubate.

Two sets of control tubes were also prepared and consisted of the U-rich synthetic groundwater. Set 1 consisted of labeled acetic acid without bacteria, whereas set 2 contained bacteria, but no acetic acid. The Si chips with biofilm were harvested under anaerobic conditions after four days. Excess adhered biofilm cells were carefully loaded onto W-coated TEM grids. Both the Si wafers and grids were freeze-dried using the technique described by Chandra & Morrison (1997) and stored in a nitrogen atmosphere prior to SIMS and TEM imaging.

High-resolution transmission electron microscopy

High-resolution transmission electron microscopy (HRTEM), analytical electron microscopy (AEM), and high-angle annular dark-field scanning transmission electron microscopy (HAADF–STEM) were conducted using a JEOL JEM2010F. The TEM specimen holders were cleaned by plasma using the Fischione Model C1020 prior to STEM analysis to minimize contamination. STEM–EDX maps were obtained using an Emispec ES Vision version 4.0 system. Drift-correction was applied during the acquisition of EDX maps to minimize the effect of instrument drift. Instrumental parameters were as follows: spherical coefficient C_s = 1.0 mm, probe sizes were 0.2 nm for high-resolution HAADF–STEM and 1.0 nm for the analyses, the collection angle of the HAADF detector was 50–110 mrad, the objective aperture size was 20 μm, and the defocus condition was ~–55 nm. The HAADF–STEM technique is an ideal method of nanoscale chemical mapping of the distribution of heavy elements on a light element matrix. The details and capabilities of HAADF–STEM analysis are further summarized in Utsunomiya & Ewing (2003).

SIMS ion imaging

Ion imaging of biofilms by secondary-ion mass spectrometry (SIMS) requires that the samples conduct electricity because the specimens are held at –4.5 kV and build up a positive charge due the impingement of the Cs^+ primary ion beam (see below). Therefore, the biofilms were grown on conductive Si wafers. Once the biofilms were freeze-dried, they were gold-coated to further enhance conductivity.

SIMS images with a spatial resolution of ~1 μm were obtained using a CAMECA 4f secondary-ion mass spectrometer in scan mode. A focused ~1 μm primary ion beam of Cs^+ accelerated at 10 kV was used to raster

the sample surface. The accelerating voltage was –4.5 kV, with the electrostatic analyzer in the secondary column set to accept –4.5 kV. Ions were detected with a Balzers SEV 1217 electron multiplier coupled with an ion-counting system, with an overall deadtime of 15 ns. The following species were detected sequentially by switching the magnetic field: $^{13}C^{14}N^-$, mass 223 (fatty acid), and $^{238}U^{16}O^-$. Typical analyses lasted approximately 10 minutes. Higher-resolution (~50 nm) SIMS images were obtained using a CAMECA NanoSIMS 50 at Washington University in St. Louis. A focused ~50 nm Cs^+ primary ion beam accelerated at 16 kV was used to raster over the sample surface, and negative secondary ions were extracted with –8 kV. Several species ($^{13}C^{14}N^-$, mass 223, and $^{238}U^{16}O^-$) were detected simultaneously with the multicollector electron-multiplier ion-counting system. Typical analyses lasted approximately 5 minutes.

Results

High-resolution transmission electron microscopy

Bright-field imaging (Fig. 1a) and energy-dispersion X-ray spectroscopy (EDX) (Fig. 1b) were used to chemically characterize the surface of the biofilm and locate the uranium-rich regions. Uranium was detected only on the surface of the bacteria (areas B and C; Fig. 1b). Flocculated grains of uranium-rich minerals in the matrix between bacteria, which were observed in experiments by Suzuki *et al.* (2002), were not observed in our experiments. Imaging and elemental mapping of the surface of the bacteria using the HAAD–STEM show that the surfaces of the bacteria contain Na, Cl, and U, in addition to C and O (Figs. 2a, b). Other elements that were also present in the groundwater, such as Mg, K, and Mn, were not detected on the

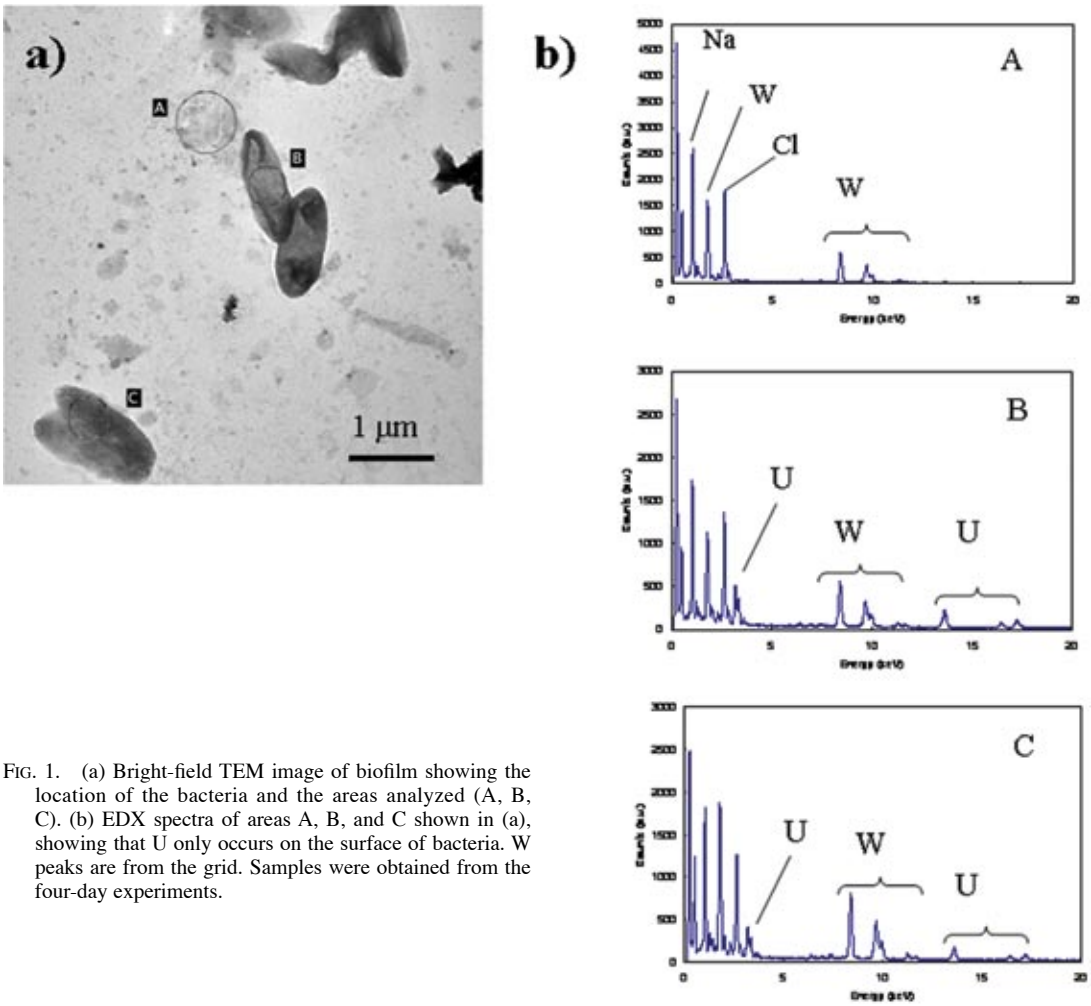

FIG. 1. (a) Bright-field TEM image of biofilm showing the location of the bacteria and the areas analyzed (A, B, C). (b) EDX spectra of areas A, B, and C shown in (a), showing that U only occurs on the surface of bacteria. W peaks are from the grid. Samples were obtained from the four-day experiments.

surfaces of the cells. High-spatial-resolution imaging of the surface of bacteria outlined in red in Figure 2a using HAAD–STEM analysis of the area reveals that U and O correlate and occur as discrete patches (Figs. 3a, b). Sodium and Cl also occur in discrete patches, but do not correlate with the U- or O-rich areas (Figs. 3a, b). Although the uranium was initially in solution as a chloride species, element-distribution maps show that U is no longer associated Cl, and there is a consistent relationship between U and O, and Na and Cl, which is consistent with precipitation of U as a uranium oxide.

High-resolution transmission electron microscopy (HRTEM) of these patches show they are crystalline and with *d* values consistent with uraninite (UO_2; Fig. 3c). However, a major concern during biomineral imaging by TEM is the extent of recrystallization (*e.g.,* Suzuki & Banfield 1999). Therefore, the minerals characterized by TEM may not represent the phases that precipitated under experimental conditions. To determine the extent of recrystallization during TEM analysis, selected-area electron-diffraction patterns (SAED) of the same area

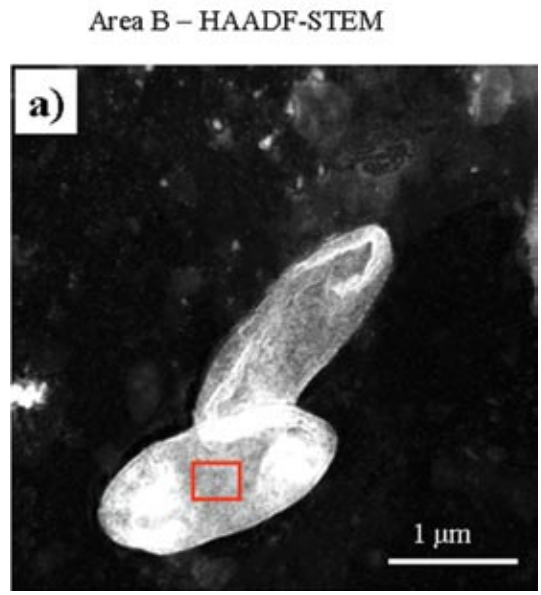

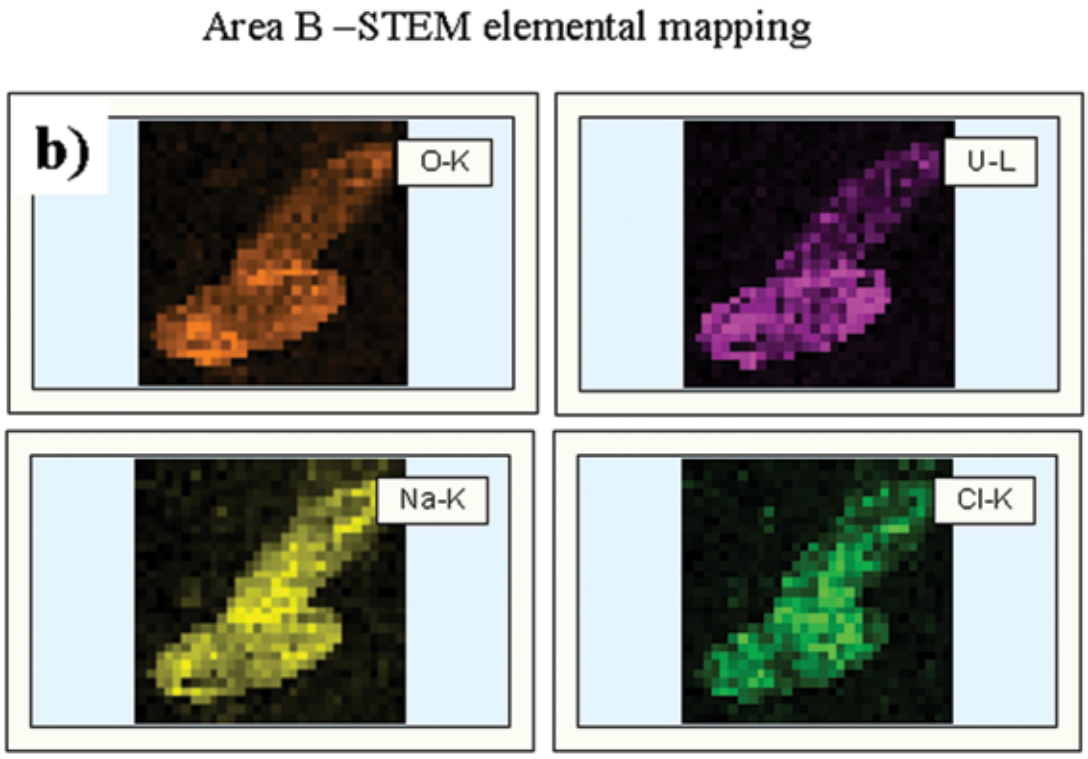

FIG. 2. (a) HAADF–STEM image of whole bacteria. (b) STEM–EDX element-distribution maps of Na, Cl, O, and U showing these elements located on the surface of the bacteria. Red box represents area selected for high-resolution (nm) HAADF–STEM analysis shown in Figure 3.

were obtained before and after HRTEM images were acquired (Fig. 4). The initial electron-diffraction pattern (Fig. 4a) was taken with an extremely low-electron-flux (~0.1 pA/cm^2) electron beam. Then the electron flux was increased to ~15 pA/cm^2 for HRTEM analysis. A second electron-diffraction pattern (Fig. 4b) was then obtained after HRTEM analysis. This SAED pattern did not change with increasing electron-dose, suggesting that recrystallization was minimal and that uraninite was likely precipitated on the surface during the experiments.

Ion imaging by SIMS

Ion imaging of the biofilm by SIMS was used to track and correlate ^{13}C-labeled acetic acid incorporation and uranium reduction. Uranium was not detected in either set of the control experiments, which suggests that the uranium remained in solution. However, SIMS imaging of the biofilms from the four-day experiments with both acetic acid and bacteria show strong correlations among $^{238}U^{16}O^-$, $^{13}C^{14}N^-$, and ^{13}C fatty acids (mass 223; Figs. 5a, b, c). Higher-resolution NanoSIMS images (Figs. 5d, e, f) show that the uranium oxide coats the surface of the bacteria. Imaging through the cell walls of the top layer of bacteria reveals that the internal components of the bacteria (Fig. 5d) are devoid of uranium oxide (Fig. 5f). These images suggest that biosorption is the dominant metal-sequestering mechanism.

The main challenge in imaging biological samples using SIMS is sample preparation because of the high vacuum required for SIMS and the hydrous nature of biological samples. A technique has been developed where cell samples are prepared using a sandwich freeze-fracture method (*e.g.,* Chandra *et al.* 1986, Chandra & Morrison 1997). The samples are prepared by sandwiching the cell cultures between the substrate and a second silicon wafer. Prior to the addition of the second silicon wafer, polystyrene beads are added to the growth medium, which protect the cells from being squashed. The silicon sandwich is then fast-frozen in supercooled isopentane and quickly transferred to liquid nitrogen. Under liquid nitrogen conditions, the silicon wafers are pried apart to fracture the cells. The silicon substrates containing the frozen-hydrated fractured cells are then transferred to a freeze-drier, dried at 183 K for 24 hours, then gold-coated to enhance electrical conductivity, which is essential for SIMS imaging (Chandra *et al.* 1986, 2000, Chandra & Morrison 1997). The advantages of this method are highlighted by the fact that cells remain unperturbed in their growth medium throughout the sampling procedure, and subcellular imaging is possible.

Although we followed the freeze-drying technique described above so that the cells remained undisturbed in their growth medium, we found that cellular fracturing was unnecessary. Using the NanoSIMS and continuous sputtering with a very-low-intensity (~0.1 pA) primary ion beam, ångström-thick layers were sequentially removed, eventually revealing the subcellular components (Figs. 5d, g, h). Ion images can be acquired throughout the sputtering processes such that a three-dimensional image of the biofilm can be compiled.

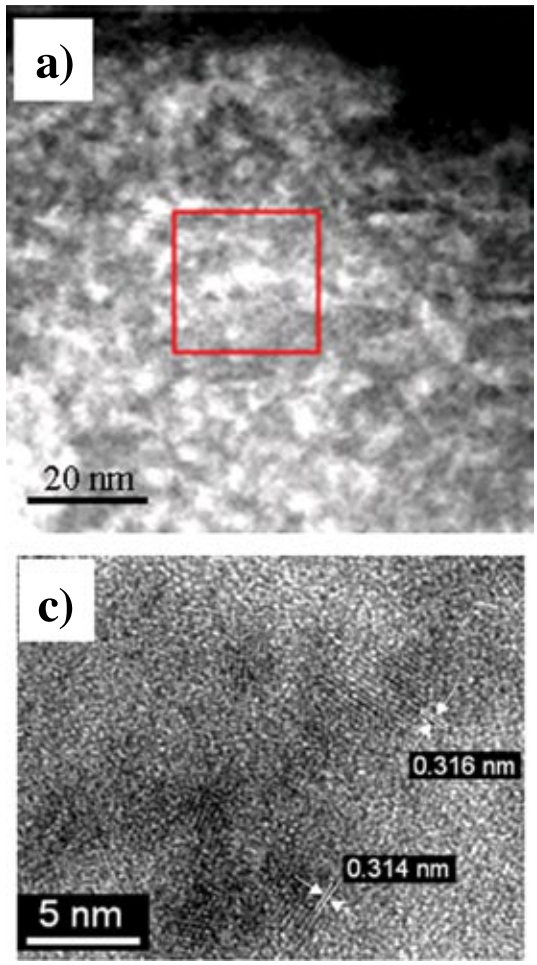

FIG. 3. (a) HAADF–STEM image of the surface of bacteria (area outlined in red, Fig. 2). (b) STEM–EDX element-distribution maps of Na, Cl, O, and U from the region outlined in (a), showing the congruency between O and U, and Na and Cl. Note that U and Cl are decoupled. (c) HRTEM image showing the size of the nanocrystals of uranium oxide on the surface of the bacteria. Numbers are *d* values, which are indicative of the mineral uraninite (UO_2). Samples were obtained from the four-day experiments.

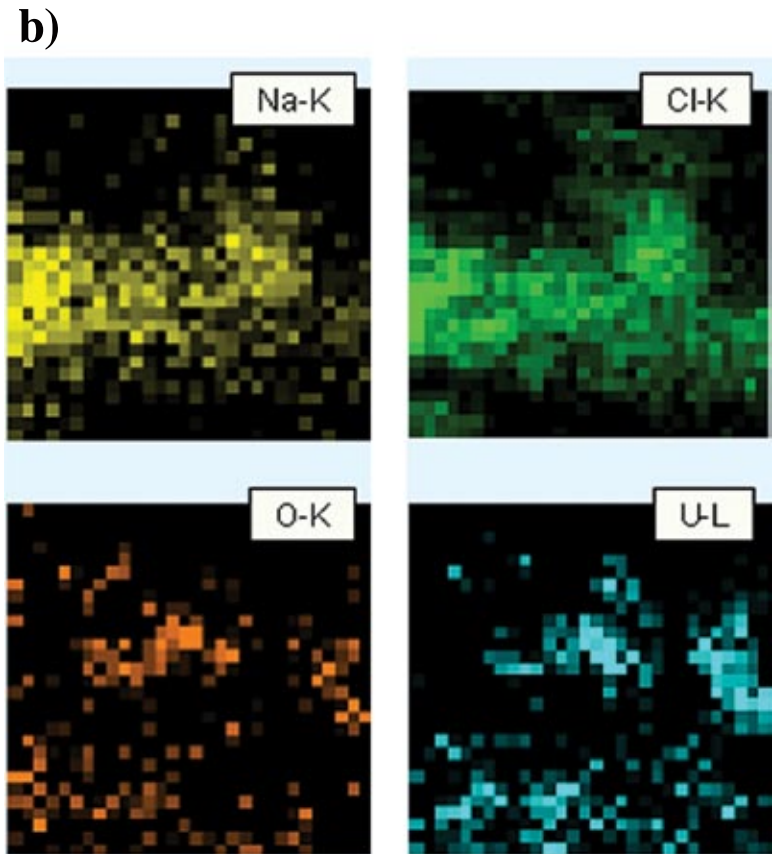

Discussion

The reduction of radionuclides in anaerobic environments is generally the result of direct enzymic reduction by bacteria (*e.g.,* Lovley *et al.* 1991, Lloyd *et al.* 2002, Suzuki *et al.* 2002). Lovley *et al.* (1991) showed experimentally, using *G. sulfurreducens* (GS–15) and ^{14}C-labeled acetate, that as cell concentrations increased, U^{4+} concentrations and $^{14}CO_2$ increased, and U^{6+} concentrations decreased. They showed that as acetate was incorporated into the growth medium, $^{14}CO_2$ was generated in direct proportion to U^{6+} reduction. Given that a small proportion of the acetate metabolized would be incorporated into the cells, they concluded that GS–15 obtained energy for growth by oxidizing acetate with the reduction of U^{6+} to U^{4+} (Lovley *et al.* 1991).

The results of our experiments are very similar to those of Lovley *et al.* (1991), Gorby & Lovley (1993), Lovley & Phillips (1992), Lloyd *et al.* (2002), and Suzuki *et al.* (2002). The ^{13}C from the ^{13}C-labeled acetic acid was incorporated into the growth medium and correlates with the uraninite, which is a U^{4+} phase. Thus *G. sulfurreducens* seems to have oxidized the acetic acid (CH_3CO_2H) while reducing U^{6+} to U^{4+} and precipitating uraninite according to the following simplified reaction:

$$CH_3CO_2H + U^{6+}Cl_3^{3+} + 4H_2O = U^{4+}O_{2\,(s)} + 2CO_{2\,(g)} + 3HCl + 4.5H_{2\,(g)} \quad [1]$$

However, previous studies, in which air-dried preparations of whole cells were viewed using TEM, showed that an electron-dense, uranium-containing precipitate, presumably uraninite (Gorby & Lovley 1993, Lovley & Phillips 1992), occurs outside the cell, whereas minor additional staining was also noted within the periplasm of the cell. These results suggest that the majority of uranium reduction (U^{4+}) is not catalyzed at the cell surface, which is in contrast to our results, where we find uranium reduction occurring only on the surface of the bacteria. Although our experiments and imaging techniques cannot confirm the exact location of the uramiun within the cell membrane (*e.g.,* outer membrane *versus* periplasm), studies by Seeliger *et al.* (1998), and Lloyd *et al.* (1999, 2002) have shown that the protein 9.6-kDa c_7 cytochrome, which is the most

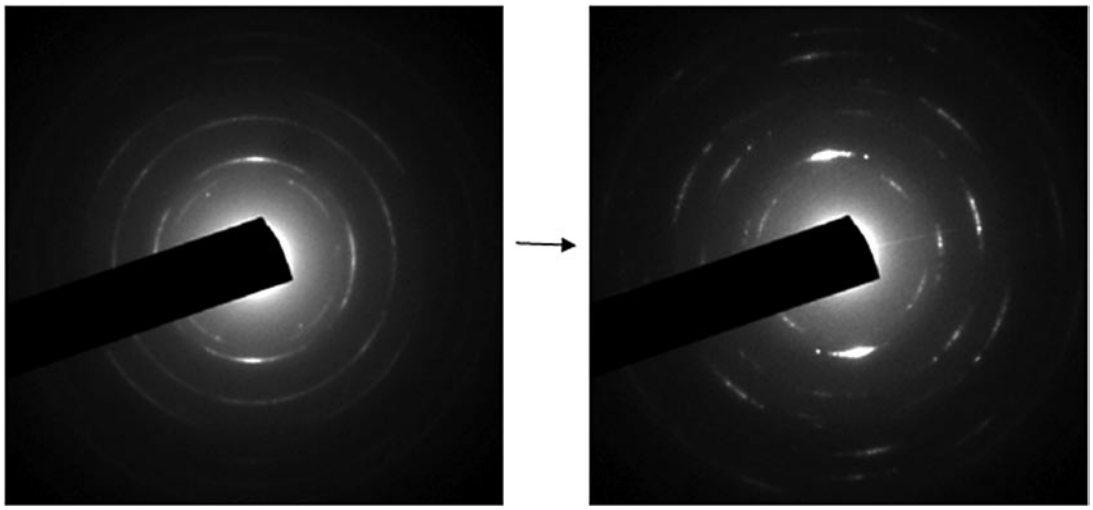

FIG. 4. Selected-area electron-diffraction patterns (SAED) collected (a) before and (b) after HRTEM analysis, showing that the biominerals that precipitated on the surface of the bacteria are stable during TEM analysis.

abundant c-type cytochrome in the periplasm of *G. sulfurreducens*, can reduce uranium *in vitro*. Therefore, at least some of the uranium in our experiments may have traversed the outer membrane and penetrated the periplasm, where it was reduced and precipitated.

Although bioprecipitation of UO_2 is well documented in the biogeochemical literature (*e.g.,* Gorby & Lovley 1993, Lovley & Phillips 1992), the presence of this structurally simple, anhydrous reduced U-rich phase is significant because thermodynamic modeling of inorganic systems and observed inorganic processes suggest that oxyhydroxide phases of uranium (U^{6+}) should have formed (Frondel 1956, Smith 1984, Wronkiewicz *et al.* 1992, Janeczek *et al.* 1993, Fayek *et al.* 1996, Chen *et al.* 1999, Finch & Murakami 1999, Jensen *et al.* 2002, Labroche *et al.* 2003a, b). Although the results of our experiments are not absolutely conclusive, they do suggest that the uraninite that is precipitated may be shielded from re-oxidation by the biofilm. This is an important result, as it suggests a mechanism for the longer time-scale sequestration of uranium, even under oxidizing conditions. However, the real mechanism is likely a complex interplay between kinetic and thermodynamic constraints, the details of which are beyond the scope of this study.

CONCLUSIONS

High-resolution transmission electron microscopy combined with nanoscale ion-imaging is a powerful technique for imaging microbial surfaces, tracking the uptake of radionuclides, and identifying the bioprecipitated mineral phases. Results from our experiments show that *G. sulfurreducens* incorporated acetic acid and reduced U^{6+} to U^{4+}, which was precipitated as uraninite on the surfaces of the bacteria. The bioprecipitation of UO_2 is significant because thermodynamic modeling of inorganic systems and observed inorganic processes suggest that uranium-poor, oxyhydroxide phases of uranium should have formed. The presence of uraninite suggests that the biofilm may have protected the uraninite from oxidation and that uranium can be immobilized for extended periods, even under the relatively oxidizing conditions of the subsurface where bacteria are active. When proper sample-preparation techniques are combined with the high spatial resolution of TEM and SIMS, detailed information on the chemical distribution and speciation of radionuclides, such as uranium, can be obtained on a scale never before achieved, allowing new insights into the mechanisms of uranium bio-accumulation and biomineral formation.

ACKNOWLEDGEMENTS

We dedicate this manuscript to Prof. Michael E. Fleet. Prof. Fleet's research couples cutting-edge geochemical and mineralogical techniques. It is at the crossroads of two disciplines that some of the most innovative research is accomplished. It was Prof. Fleet's early SIMS research that provided the impetus for the first author to pursue a career that heavily relies on SIMS.

Research sponsored by the Division of Chemical Sciences, Geosciences, Biosciences, Office of Basic Energy Sciences, U.S. Dept. of Energy, under contract DE–AC05–00OR22725 with Oak Ridge National

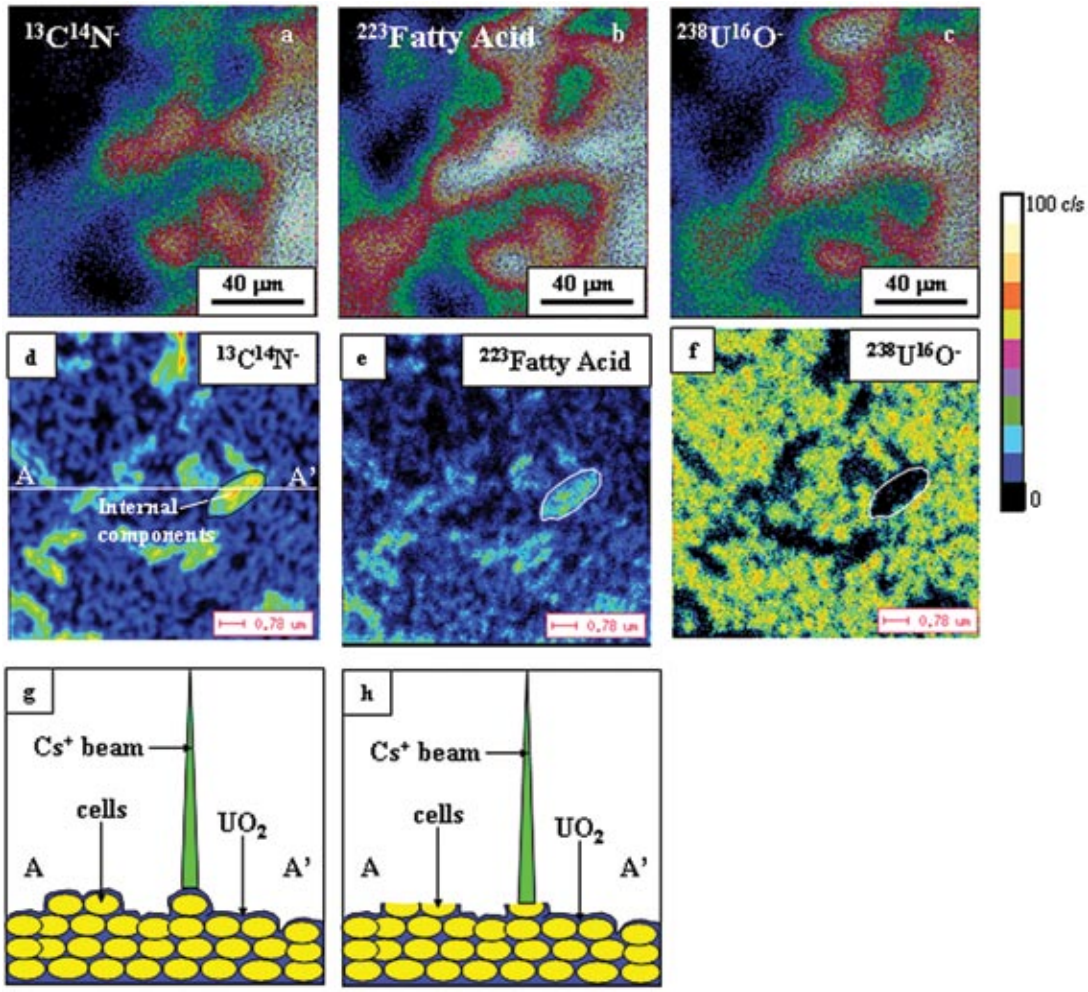

FIG. 5. Micro-SIMS image of (a) $^{13}C^{14}N$ molecule and (b) fatty acids marking the location of *Geobacter* biofilm that grew on Si wafers. (c) The $^{238}U^{16}O$ maps the location of the uranium. These images show that where there are no bacteria, there is also no uranium oxide. Note that the individual bacteria are not spatially resolved. (d) and (e) NanoSIMS image of the same sample showing individual bacteria (outlined). The biofilm consists of several layers of cells. Imaging through the cell walls of the top layer of bacteria reveals their internal components. (f) NanoSIMS image showing the exact location of $^{238}U^{16}O$ relative to the cell walls (outlined in white). The central parts of the cell are devoid of $^{238}U^{16}O$. Samples were obtained from the four-day experiments. Color bar shows the relative intensity of the ion signal in counts per second (c/s), which correlates with the concentration of molecules detected. (g) and (h) Schematic cross-sections through A–A' shown in (d) illustrating how the NanoSIMS can sputter through cellular surfaces, thus allowing subcellular imaging.

Laboratory, managed and operated by UT–Battelle, LLC, grant DE–FC02–96ER62278, Office of Biological and Environmental Research of the Office of Science, Natural and Accelerated Bioremediation Research (NABIR) Program, U.S. Dept. of Energy, and Environmental Management Science Program (DE–FG07–97ER14816 to RCE). We thank Mr. François Hillion for his help in acquiring the NanoSIMS images and Dr. Yuri A. Gorby for providing the bacteria cultures.

REFERENCES

ABDELOUAS, A., LUTZE, W. & NUTTALL, H.E. (1999): Oxidative dissolution of uraninite precipitated on Navajo sandstone. *J. Contam. Hydrol.* **36**, 353-375.

ANDRES, Y., MACCORDICK, J. & HURBERT, J.C. (1993): Adsorption of several actinides (Th, U) and lanthanides (La, Eu, Yb) ions by *Mycobacterium smegmatis*. *Appl. Microbiol. Biotechnol.* **39**, 413-417.

CHANDRA, S. & MORRISON, G.H. (1997): Evaluation of fracture planes and cell morphology in complementary fractures of cultured cells in the frozen-hydrated state by field-emission secondary electron microscopy: feasibility from ion localization and fluorescence imaging studies. *J. Microsc.* **186**, 232–245.

_____, _____ & WOLCOTT, C.C. (1986): Imaging intracellular elemental distribution and ion fluxes in cultured cells using ion microscopy: a freeze-fracture methodology. *J. Microsc.* **144**, 15–37.

_____, SMITH, D.R. & MORRISON, G.H. (2000): Subcellular imaging by dynamic SIMS ion microscopy. *Anal. Chem.* **72**, 104-114.

CHEN, FANRONG, EWING, R.C. & CLARK, S.B. (1999): The Gibbs free energies and enthalpies of formation of U^{6+} phases: an empirical method of prediction. *Am. Mineral.* **84**, 650-664.

FAYEK, M., KYSER, T.K., EWING, R.C. & MILLER, M.L. (1996): Geochemical consequences of uraninite–water interaction in an oxidizing environment. *Mater. Res. Soc., Symp.Proc.* **412**, 1201-1208.

FEIN, J.B., DAUGHNEY, C.J., YEE, N. & DAVIS, T.A. (1997): A chemical equilibrium model for metal adsorption onto bacterial surfaces. *Geochim. Cosmochim. Acta* **61**, 3319-3328.

FERRIS, F.G., FYFE, W.S. & BEVERIDGE, T.J. (1988): Metallic ion binding by *Bacillus subtilis*: implications for the fossilization of microorganisms. *Geology* **16**, 149-152.

FINCH, R.J. & MURAKAMI, T. (1999): Systematics and paragenesis of uranium minerals. *In* Uranium: Mineralogy, Geochemistry and the Environment (P.C. Burns & R.J. Finch, eds.). *Rev. Mineral.* **38**, 91-179.

FOWLE, D.A. & FEIN, J.B. (2001): Quantifying the effects of *Bacillis subtilis* cell walls on the precipitation of copper hydroxide from aqueous solution. *Geomicrobiol. J.* **18**, 77-91.

_____, _____ & MARTIN, A.M. (2000): Experimental study of uranyl adsorption onto *Bacillus subtilis*. *Environ. Sci. Technol.* **34**, 3737-3741.

FRONDEL, C. (1956): The mineralogical composition of gummite. *Am. Mineral.* **41**, 539-568.

GORBY, Y.A. & LOVLEY, D.A. (1993): Enzymatic uranium precipitation. *Environ. Sci. Technol.* **26**, 205-207.

HINDIÉ, E. (1997): Subcellular localization of isotopes and labelled molecules by SIMS. *Proc. SIMS* **XI** (*Orlando*), 113.

JANECZEK, J., EWING, R.C. & THOMAS, L.E. (1993): Oxidation of uraninite: does tetragonal U_3O_7 occur in nature? *J. Nucl. Mater.* **207**, 176-191.

JENSEN, K.A., PALENIK, C.S. & EWING, R.C. (2002): U^{6+} phases in the weathering zone of the Bangombe U-deposit: observed and predicted mineralogy. *Radiochim. Acta* **90**, 761-769.

KELLY, S.D., KEMNER, K.M., FEIN, J.B., FOWLE, D.A., BOYANOV, M.I., BUNKER, B.A. & YEE, N. (2002): X-ray absorption fine structure determination of pH-dependent U-bacterial cell wall interactions. *Geochim. Cosmochim. Acta* **66**, 3855-3871.

KONHAUSER, K.O., SCHULTZE-LAM, S., FERRIS, F.G., FYFE, W.S., LONGSTAFFE, F.J. & BEVERIDGE, T.J. (1994): Mineral precipitation by epilithic biofilms in the Speed River, Ontario, Canada. *Appl. Environ. Microbiol.* **60**, 549-553.

LABROCHE, D., DUGNE, O. & CHATILLON, C. (2003a): Thermodynamics of the O–U system. I. Oxygen chemical potential critical assessment in the UO_2–U_3O_8 composition range. *J. Nucl. Mater.* **312**, 21-49.

_____, _____ & _____ (2003b): Thermodynamics of the O–U system. II. Critical assessment of the stability and composition range of the oxides UO_{2+x}, U_4O_{9-y}, and U_3O_{8-z}. *J. Nucl. Mater.* **312**, 50-66.

LECHENE, C., HILLION, F. & MROZ, E. (2003): Isotope ratio imaging of biological tissues with multi-isotope imaging mass spectrometry (MIMS). *Proc. SIMS* **XIV** (*San Diego*).

LLOYD, J.R., BLUNT-HARRIS, E.L. & LOVLEY, D.R. (1999): The periplasmic 9,6 kDa c-type cytochrome of Geobacter sulfurreducens is not an electron shuttle to Fe(III). *J. Bacteriol.* **181**, 7647-7649.

_____, CHESNES, J., GLASAUER, S., BUNKER, D.J., LIVENS, F.R. & LOVLEY, D.R. (2002): Reduction of actinides and fission products by Fe(III)-reducing bacteria. *Geomicrobiol. J.* **19**, 103-120.

LOVLEY, D.R. & PHILLIPS, E.J.P. (1988): Novel mode of microbial energy metabolism: organic carbon oxidation coupled to dissimilatory reduction of iron and manganese. *Appl. Environ. Microbiol.* **54**, 1472-1480.

_____ & _____ (1992): Reduction of uranium by *Desulfovibrio desulfuricans*. *Appl. Environ. Microbiol.* **58**, 85-93.

_____, _____, GORBY, Y.A. & LANDA, E.R. (1991): Microbial reduction of uranium. *Nature* **350**, 413-416.

MARKOVIC, M., PARKOVIC, N. & PARKOVIC, N.D. (1988): Precipitation of ammonium uranyl phosphate trihydrate solubility and structural comparison with alkali uranyl (2+) phosphate. *J. Res. Natl. Bureau Stand. USA* **93**, 557-563.

PACHOLSKI, M.L. & WINOGRAD, N. (1999): Imaging with mass spectrometry. *Chem. Rev.* **99**, 2977-3006.

RAMSEYER, G.O., BRENNA, J.T., MORRISON G.H. & SCHWARTZ, R. (1984): Elemental isotopic abundance determinations of

magnesium in biological materials by secondary ion mass spectrometry. *Anal. Chem.* **56**, 402-407.

SCHARER, J.M. & BYERLEY, J.J. (1989): Aspects of uranium adsorption by microorganisms. *Hydrometallurgy* **21**, 319-329.

SEELIGER, S., CORD-RUWISCH, R. & SCHINK, B. (1998): A periplasmic and extracellular c-type cytochrome of *Geobacter sulfurreducens* acts as a ferric ion reductase and as an electron carrier to other acceptors or to partner bacteria. *J. Bacteriol.* **180**, 3686-3691.

SMITH, D.K. (1984): Uranium mineralogy. *In* Uranium Geochemistry, Mineralogy, Geology, Exploration and Resources (B. De Vivo, F. Ippolito, G. Capaldi & P.R. Simpson, eds.). Stephen Austin/Hartford Press, London, U.K. (43-88).

SOUTHAM, G. (2000): Bacterial surface-mediated mineral formation. *In* Environmnetal Microbe–Metal Interactions (D.R. Lovley, ed.).). ASM Press, Washington, D.C. (257-277).

SUZUKI, Y. & BANFIELD, J.F. (1999): Geomicrobiology of uranium. *In* Uranium: Mineralogy, Geochemistry and the Environment (P.C. Burns & R.J. Finch, eds.). *Rev. Mineral.* **38**, 393-432.

_____, KELLY, S.D., KEMNER, K.M. & BANFIELD, J.F. (2002): Nanometre-size products of uranium bioreduction. *Nature* **419**, 134.

TSEZOS, M. & VOLESKY, B. (1982): The mechanism of uranium biosorption by *Rhizopus arrhizus*. *Biotechnol. Bioengineer.* **24**, 385-401.

UTSUNOMIYA, S. & EWING, R.C. (2003): Application of high-angle annular dark field scanning transmission electron microscopy, scanning transmission electron microscopy – energy dispersive X-ray spectrometry, and energy-filtered transmission electron microscopy to the characterization of nanoparticles in the environment. *Environ. Sci. Tech.* **37**, 786-791.

WRONKIEWICZ, D.J., BATES, J.K., GERDING, T.J., VELECKIS, E. & TANI, B.S. (1992): Uranium release and secondary phase formation during unsaturated testing of UO_2 at 90°C. *J. Nucl. Mater.* **190**, 107-127.

Received January 25, 2005, revised manuscript accepted July 3, 2005.